Article:

Collier, N.C., Heyes, D.W., Butcher, E.J. et al. (10 more authors) (2019) Gaseous carbonation of cementitious backfill for geological disposal of radioactive waste : Nirex Reference Vault Backfill. Applied Geochemistry, 106. pp. 120-133. ISSN 0883-2927

https://doi.org/10.1016/j.apgeochem.2019.04.020

Gaseous carbonation of cementitious backfill for geological disposal of radioactive waste: Nirex Reference Vault Backfill

Nicholas C Collier[a], David W Heyes[a], Ed J Butcher[a,*], Jason Borwick[a], Antoni E Milodowski[b], Lorraine P Field[b], Simon J Kemp[b], Ian Mounteney[b], Susan A Bernal[c,d], Claire L Corkhill[c], Neil C Hyatt[c], John L Provis[c], Leon Black[d]

[a] National Nuclear Laboratory, Havelock Rd, Derwent Howe, Workington, CA14 3YQ, UK.

[b] British Geological Survey, Environmental Science Centre, Nicker Hill, Keyworth, Nottingham, NG12 5GG, UK.

[c] NucleUS Immobilisation Science Laboratory, Department of Materials Science and Engineering, The University of Sheffield, Mappin Street, Sheffield, S1 3JD, UK.

[d] School of Civil Engineering, University of Leeds, Woodhouse Lane, Leeds LS2 9JT.

* Corresponding author. Email ed.j.butcher@nnl.co.uk.

Keywords: NRVB, Nirex Reference Vault Backfill, carbon dioxide, carbonation, cement, intermediate level waste, immobilization, radioactive, nuclear.

Abstract

The ability of Nirex Reference Vault Backfill (NRVB), a cement backfill material, to capture carbon dioxide from Intermediate Level Radioactive waste packages after repository backfilling, has been assessed. Large-scale trials assessed the physical and chemical reaction of carbon dioxide with the hardened backfill grout. A carbonation front, radial in nature, was observed extending into the grout and three distinct regions were identified in the hardened grouts. A carbonated region, a carbonation front, and a partially carbonated zone were discerned. Potassium, and to a lesser extent sodium, were concentrated in the carbonated region just behind of the main reaction front. The area just ahead of the carbonation front was enriched in both sulphur and aluminium, while sulphur was found to be depleted from the carbonated material behind the main reaction front. Within the main carbonated region, virtually all of the hydrated cement phases were found to be carbonated, and carbonation extended throughout the grout, even within material indicated by phenolphthalein solution to be uncarbonated. Importantly, carbonation was observed to impact both the mineral assemblage and porosity of the cement backfill; it is therefore important to understand these characteristics in terms of the long term evolution of NRVB and its groundwater buffering safety function within the geological disposal facility near-field.

1. Introduction

Geological disposal in an engineered facility underground is the UK Government's policy for disposal of higher activity radioactive waste. [Department of Energy and Climate Change, 2014]. Such geological disposal facilities (GDFs) or repositories are based on the use of a multi barrier containment approach, which involves the application of engineered barriers, working in combination with natural geological features, to reduce the rate of radionuclide release to the biosphere. In the UK, an illustrative concept for disposal of Intermediate Level Waste (ILW) in a fractured crystalline rock (e.g. granitic), is that packages of grouted waste will be emplaced in sub-surface vaults and surrounded with a Portland cement-based backfill called Nirex Reference Vault Backfill (NRVB) [Pusch, 2017].

The bulk of gaseous emissions from ILW packages are expected to be hydrogen (H_2), mainly produced from the corrosion of metallic waste products and methane (CH_4) and carbon dioxide (CO_2), produced *via* the microbial degradation of organic waste materials under anaerobic or aerobic conditions [Radioactive Waste Management Limited, 2016a; Amec Foster Wheeler, 2017]. A small proportion of the gas produced would include tritium (^3H), ^{14}C species (including $^{14}CH_4$ and $^{14}CO_2$) and radon (Rn-222). It is desired that, after backfilling, either the cementitious material in the waste packages, or in the backfill, would capture any waste CO_2 (including $^{14}CO_2$), thus retarding its egress to the geosphere [Hoch et al., 2016]. .

In ordinary Portland cements used for construction purposes, CO_2 from the atmosphere diffuses through gas-filled pores and dissolves into the pore solution forming aqueous HCO_3^-. The uptake of acidic CO_2 into the alkaline pore solution reduces the internal pH of the binder, and the dissolved carbonate also reacts with calcium-rich hydration products present in the matrix, mainly with portlandite ($Ca(OH)_2$), calcium silicate hydrate (C-S-H[1]) and the various calcium aluminate hydrates present, to form solid calcium carbonates, silica gel and hydrated aluminium and iron oxides [Johannesson and Utgenannt, 2001; Živica and Bajza, 2001;

---

[1] Calcium silicate hydrate is the principal binding phase in Portland cement based systems. C, S and H indicate the oxides of calcium, silicon and hydrogen respectively, while the hyphens reflect the variable composition of the material.

Fernández-Bertos *et al.*, 2004].

The effect of carbonation on the mineralogy and porosity, are the two most important characteristics that influence the ability of a cementitious backfill grout to buffer groundwater to high pH (as desired to retard release of radionuclides to the geosphere), (cf. Nuclear Decommissioning Authority. 2010; Wilson et al., 2017), and the effect has not been fully elucidated. The reaction of CO_2 in the gas phase with typical waste encapsulation grouts and NRVB, in unsaturated conditions, has previously been studied in laboratory experiments e.g. Harris *et al.*, [2003a; 2003b] and ; Sun [2010] Carbonation was considered to be associated principally with the portlandite and C-S-H components, facilitated by the dissolution of CO_2 into films of water condensing on the cement phases and consequently, the reaction rate is strongly influenced by relative humidity [Bamforth et al., [2012], More recently, experimental studies simulating saturated repository environments have been undertaken to examine the effect of carbonation on gas-transport properties of NRVB [Rochelle et al., 2013; Purser et al., 2015]. There has also been significant interest in studying cement carbonation in deep saline brine groundwater environments to evaluate the performance of cementitious well seals in relation to the geological sequestration of CO_2 [e.g. Kutchko et al., 2007; Rochelle et al., 2009; Wilson et al., 2011; Rochelle and Milodowski, 2013]. Natural analogue studies provide further insights into the long-term effects of carbonation on cementitious materials [Milodowski et al., 2011; Pitty and Alexander, 2011], and indicate that both the processes and degree of carbonation depend upon the geological environment and the partial pressure of CO_2 in the groundwater [Bamforth et al., 2012]. However further information is required to understand this degradation mechanism in the context of the post-closure performance of a GDF. We report here on detailed experimental studies investigating the reaction of gaseous CO_2 with hardened NRVB to support understanding of the backfill material following closure of the GDF.

It is important to revisit the chemistry and engineering performance of NRVB at this time, as the understanding of its role and function within a GDF have evolved since its initial formulation as the UK opens its siting process for such a facility

2. Experimental

2.1 Materials

Nirex Reference Vault Backfill (NRVB) was formulated according to [Francis *et al.*, 1997] using Ribblesdale Sellafield specification Portland Cement (Hanson Cement) [Cann and Orr, 2010], limestone flour (Tendley Quarries [BSI, 2005]) and hydrated lime (Limbux hydrated lime supplied by Tarmac Buxton Lime and Cement [BSI, 2015]). Characterisation of each of these materials (e.g. particle size, surface area, composition etc. are provided in Vasconcelos et al. (2018)). The formulation of the NRVB paste is shown in Table 1; the overall water to solids ratio (w/s) was 0.55.

Table 1. Formulation of the Nirex Reference Vault Backfill (NRVB) as specified by Francis *et al.*, 1997, and used in the current work

Components	**Mass** (g)	**Paste Proportion** (wt.%)	**Solids Proportion** (wt.%)
Ordinary Portland cement	450	26.01	40.36
Limestone flour	495	28.61	44.39
Hydrated lime	170	9.83	15.25
Water	615	35.55	-
Total	1730	100	100

2.2 Large-scale trial

Powders sufficient to produce a 500 L batch of grout were weighed and then added to the desired weight of water at a controlled rate over a 25 minute period into a British Nuclear Fuels Ltd (BNFL) grout mixer (an impeller in-vessel medium shear mixer, with a 500 litre capacity as used in the Sellafield Wastes Encapsulation plant (WEP)) and then mixed for a further 15 minutes. The grout was poured into a bespoke 400 L stainless steel curing vessel (Figure 1). The vessel had an internal diameter of 790 mm, an internal height of 780 mm, and incorporated a stainless steel ILW drum lid (with a standard sintered metal vent at the centre of the lid) fixed inside.

A sealed compartment located directly below the vent provided a gas-tight reservoir from which the CO_2 was emitted, this was designed to simulate the arrangement of ILW drums, releasing gas through the vent in the GDF. Before the 400L vessel was filled with grout, the inside faces were roughened, to provide better adhesion between the backfill and the vessel, and reduce the risk of gas flow between the sample and the vessel. After filling with the NRVB, the interface between the top surface of the NRVB and the vessel was filled with a beading of epoxy resin-based concrete bonding material to ensure good adhesion between the grout and the walls of the vessel (and hence reduce the pathways available for the CO_2 to flow around the grout). The vessel was then filled with 302 L of grout to cover the drum vent and form an interface with the drum lid; this simulated the backfilling of a GDF vault filled with ILW containers. The sample was sealed and cured at 40°C represent potential GDF conditions for 28 days. After this period the internal gas reservoirs were filled with CO_2 (99.8 % purity) to 0.15 MPa from an external gas bottle through a connection in the base of the vessel and into the reservoir. CO_2 pressure was measured at the gas inlet reservoir throughout, and gas consumption was calculated from pressure changes. The carbonation trial was performed at 30°C and autogenous relative humidity (RH); temperature and pressure were recorded for the duration. These conditions are designed to be comparable to those which may occur in a GDF [Radioactive Waste Management, 2016b]. The vessel was fitted with a carbon dioxide sensor in the external lid of the 400 L vessel to detect any release of CO_2 from the top surface of the grout, which would indicate either premature material degradation *e.g.* by cracking, or CO_2 permeation through the whole depth of the grout.

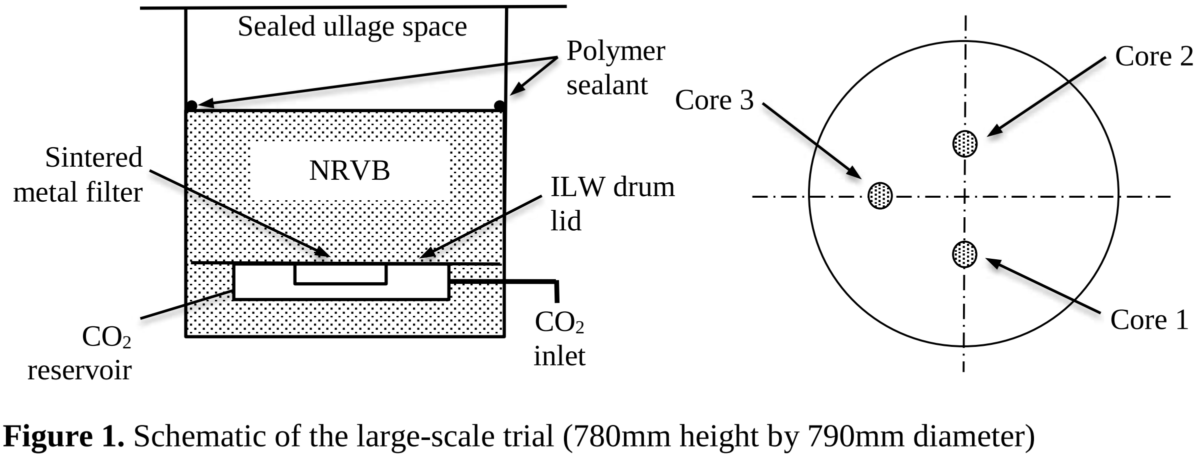

Figure 1. Schematic of the large-scale trial (780mm height by 790mm diameter)

equipment layout and a plan view of post experimental core locations.

After almost 2 years of curing and exposure to CO_2, the trial was terminated and three 48 mm diameter cores were drilled (using a single barrel corer) perpendicularly to the top surface and through the full thickness of the grout until the embedded steel ILW drum lid was reached (Fig. 1). Directly after removal, each core was placed and sealed in an argon-purged polythene sleeve, and then double bagged in a second polythene sleeve. This was performed to preserve the cores and prevent additional atmospheric. Water was used minimally for cooling and lubrication fluid during the drilling process carbonation prior to analysis. After coring, samples were sprayed with a solution of 0.2% phenolphthalein in denatured ethanol, and photographed to allow areas of bulk carbonation to be visually identified.

2.4 Analytical methods

Thermogravimetric Analysis (TGA) and Differential Scanning Calorimetry (DSC) were performed using a Netzsch STA409PC Simultaneous Thermal Analyser, using ~30 mg samples in a nitrogen atmosphere, heated from 50 to 1000°C at 10°C/min. For permeability testing, a Temco MP-402 ‘mini’- or ‘probe-permeameter’ was used. Measurements were made on the cut flat face of one half of the intact cement cores in a horizontal orientation. Flow rate and pressure were recorded and permeability was calculated. Measurements were repeated several times at the same spot and the mean was taken as the representative permeability. Measurements were recorded at various points along the length of each core at intervals of ~10 – 20 mm apart.

Selected thin sections of each core were carbon coated (~25 nm layer) and then examined using backscattered scanning electron imaging (BSEM) and energy-dispersive X-ray microanalysis (EDXA) elemental mapping. The locations of the thin section sampling points are shown in Figure 2. This was performed using an FEI QUANTA 600 environmental scanning electron microscope (ESEM) equipped with an Oxford Instruments INCA Energy 450 EDXA system. Semi-quantitative EDXA point analyses were recorded from selected X-ray mapped areas to aid phase differentiation and identification, and processed using the inbuilt “standardless” calibration Oxford Energy INCA Suite Version 4.15 (2009) software package.

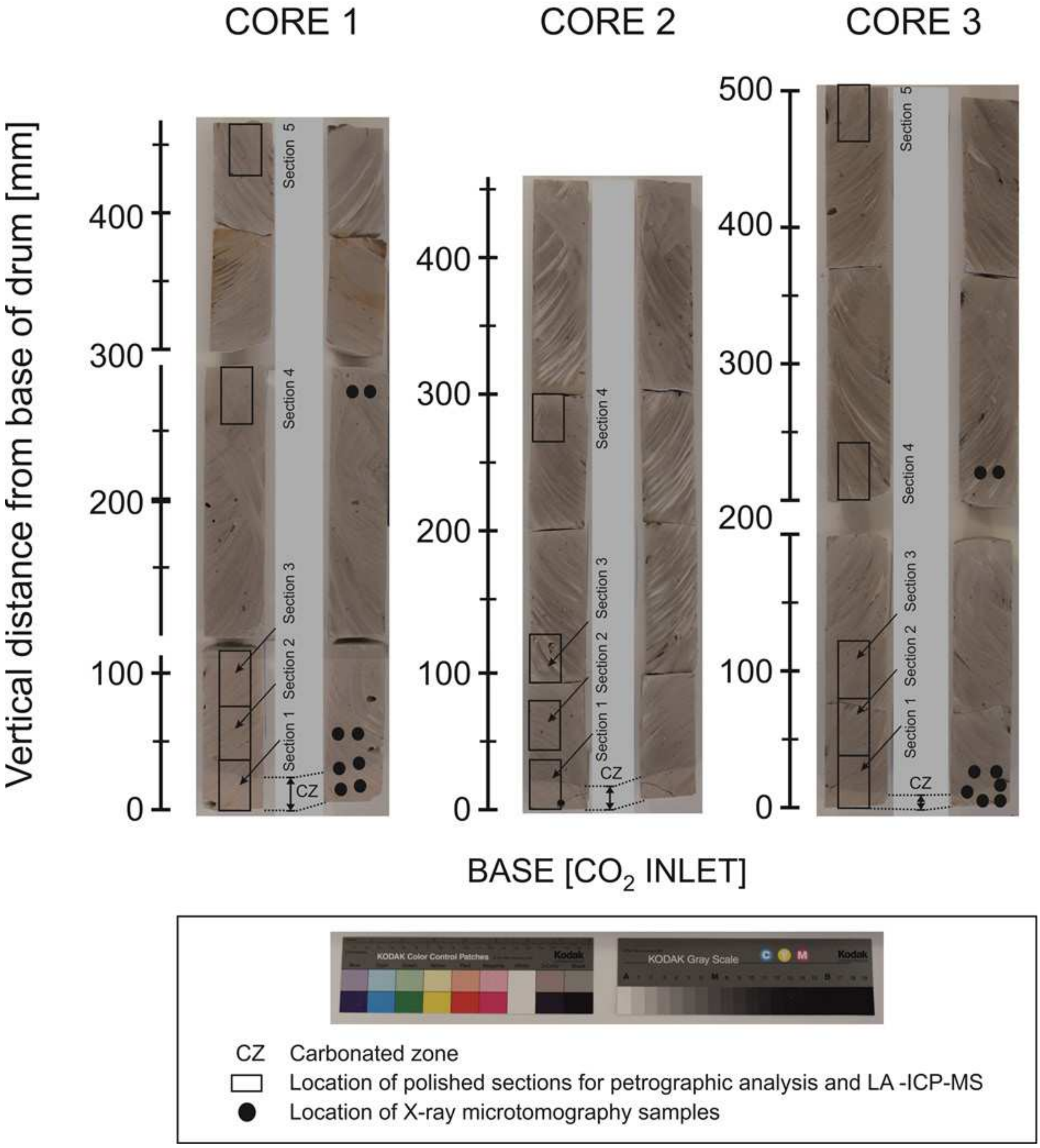

Figure 2. Photographs of the longitudinally-sliced cored samples, showing the sampling locations for petrographic thin sections, LA-ICP-MS and X-ray microtomography

Laser ablation-inductively coupled-mass spectroscopy (LA-ICP-MS) was performed using an Agilent 4500 ICP-MS, combined with a laser ablation function, on 1 mm thick samples. Measurements were carried out in the X-ray imaging facility at the University of Manchester (MXIF) using the Nikon Metris 225/320 kV Custom Bay instrument, with a 225 kV source and a PerkinElmer 2000 × 2000 pixel 16-bit amorphous silicon flat panel detector (Figure 7). The scans were collected using a tungsten target with a voltage of 70 kV and current of 170 μA, the beam was not filtered, and the exposure time per frame was 1 s. A total of 2001 projections through a full 360° rotation with 1 frame/projection were collected with a pixel size of 5 × 5 µm (resulting in a reconstructed voxel size of 5 × 5 × 5 µm). The results were acquired using the Nikon Inspect-X software, and the projections were reconstructed using Nikon CT-Pro. Beam hardening corrections (level 2 out of 6) and noise reduction (level 2 out of 6) were used while reconstructing. [Provis *et al.*, 2012]. Raman and Fourier Transform Infra-Red (FTIR) spectroscopy were both used to study material either side of a visible carbonation front. Raman spectra were recorded using a Renishaw System 2000 Raman spectrometer fitted with an Ar^+ laser (514.5 nm). Twenty spectra were accumulated, with a 10 second acquisition time, typically over the wavenumber range 200 to 1200 cm^{-1}, and samples were left under the laser light for up to 20 minutes prior to collection of the spectra to “photobleach” and reduce fluorescence [Richardson et al., 2010]. For X-ray diffraction (XRD), samples were finely-ground under acetone with 10% corundum (Al_2O_3) as an internal reference to allow validation of quantification results. XRD was carried out using a PANalytical X’Pert Pro series diffractometer equipped with a cobalt target tube, X-Celerator detector and operated at 45 kV and 40 mA. The powder samples were scanned from 4.5 - 85° 2θat a scan rate of 2.76° 2θ/minute. Quantification was achieved using the Rietveld refinement technique (*e.g.* Snyder and Bish [1989]) using PANalytical HighScore Plus software together with the Inorganic Crystal Structure Database (ICSD, 2014).

3. Results and Discussion

3.1 Carbonation front and visual characteristics

Staining (later confirmed by micro-focus techniques described in the characterisation sections below) was used to identify three distinct regions within each core of hardened NRVB: i) uncarbonated; ii) partially carbonated; and iii) carbonated regions. The partially carbonated region was observed as a distinct interface between uncarbonated and carbonated material, and was likely to be where a carbonation front was located; these three regions are each analysed in detail below. For each core, the assignment of uncarbonated, partially carbonated and carbonated regions was made based on the results obtained using phenolphthalein staining. Phenolphthalein staining was also used to measure the depth of carbonation in each of the three cores; the average depth was measured to be 26.8 mm, 21.5 mm and 11.8 mm for Core 1, 2 and 3, respectively (these were obtained by averaging between 6 and 8 measurements each).

3.2 Micropermeametry

The permeability, measured along longitudinal profiles through the three cores, varied between 0.12 and 1.07 (1σ ±0.02) mD (Table 2). These values were close to the lower limit of detection of the instrument, thus it was difficult to identify any distinct trends. However, a number of observations could be made. The permeability of the uncarbonated cement varied mostly between 0.12 and 0.26 (1σ ±0.02) mD. No relationship was observed between permeability and distance along the core, other than in the bottom 1-2 cm of each core (within the carbonation zones) where it was significantly higher, particularly for cores 1 and 3. Not only did the carbonation cause an increase in the permeability, but the texture of the grout was observed to become harder and discoloured; altering from a light grey to pale-beige colour, with a porcelaneous appearance in the carbonated zones in all cores (Figure 2)..

Table 2. Micropermeametry results

Vertical Position[a] (mm)	**Intrinsic permeability** (mD)		
	1	2	3
440	0.24	0.19	0.23
420	0.21	0.12	0.22
400	0.18	0.26	0.21
380	0.18	0.12	0.20
360	0.16	0.14	0.19
340-350	0.17	0.15	0.21
320-330	0.15	0.22	0.21
300-310	0.16	0.23	0.23
290-300	0.18	0.26	0.20
270-280	0.24	0.26	0.20
250-260	0.23	0.12	0.20
230-240	0.20	0.20	0.21
210-220	0.20	0.15	0.24
180-200	0.17	-	0.23
160-180	0.22	0.18	0.15

140-160	0.23	0.14	0.20
120-140	0.21	0.19	0.17
90-120	0.24	0.13	0.18
110-90	0.17	0.20	0.18
60-90	0.16	0.20	0.17
50-60	0.16	0.19	0.19
40-50	0.17	0.18	0.17
30-40	0.15	0.20	0.19
20-30	0.78	0.19	0.17
10-20	0.72	0.26	0.19
10			1.07

Notes. [a] – from base of core. Shading indicates carbonation based on Phenolphthalein staining. Instrumental uncertainty (1σ) = ±0.02 mD for permeability values ≤1 mD.

3.3 Acid digestion and LA-ICP-MS

The total elemental concentrations determined by acid digestion are shown in Figure 3 (Ca is not shown here due to the very high concentration of ~3 x 10^5 ppm). The concentrations of Al, Fe, Mg and Si were similar in each of the regions, indicating that if migration of these elements occurs during carbonation, it is likely to be only over short distances, as shown in Figure 4. Compared to the uncarbonated region, the carbonated and partially carbonated regions appeared to be relatively enriched in Na and K, and the carbonated region was depleted in S.

The concentrations of Sr and Ni were higher in the carbonated region than in the uncarbonated material (although this was a small difference for Sr, Fig. 2). The Ni concentration was greatest in the carbonated region; Ni sorbed to C-S-H may be released during carbonation of this phase; Ni has been reported to show very limited incorporation into calcite [Hoffmann and Stipp, 1998]. The elevated concentration of Sr in the carbonated region is likely to be due to co-precipitation with Ca and incorporation (by solid-solution) in $CaCO_3$, which is precipitated in pores during the carbonation reaction [Shafique *et al.*, 1998]. The concentration of metals is also likely to be higher in pore space filled with secondary precipitated $CaCO_3$ [Lange *et al.*, 1997]. Within error there was no difference in the concentration of the other minor and trace elements (Ba, Cr, Cu, Mn, Ti, V, Zn and Zr) between each region.

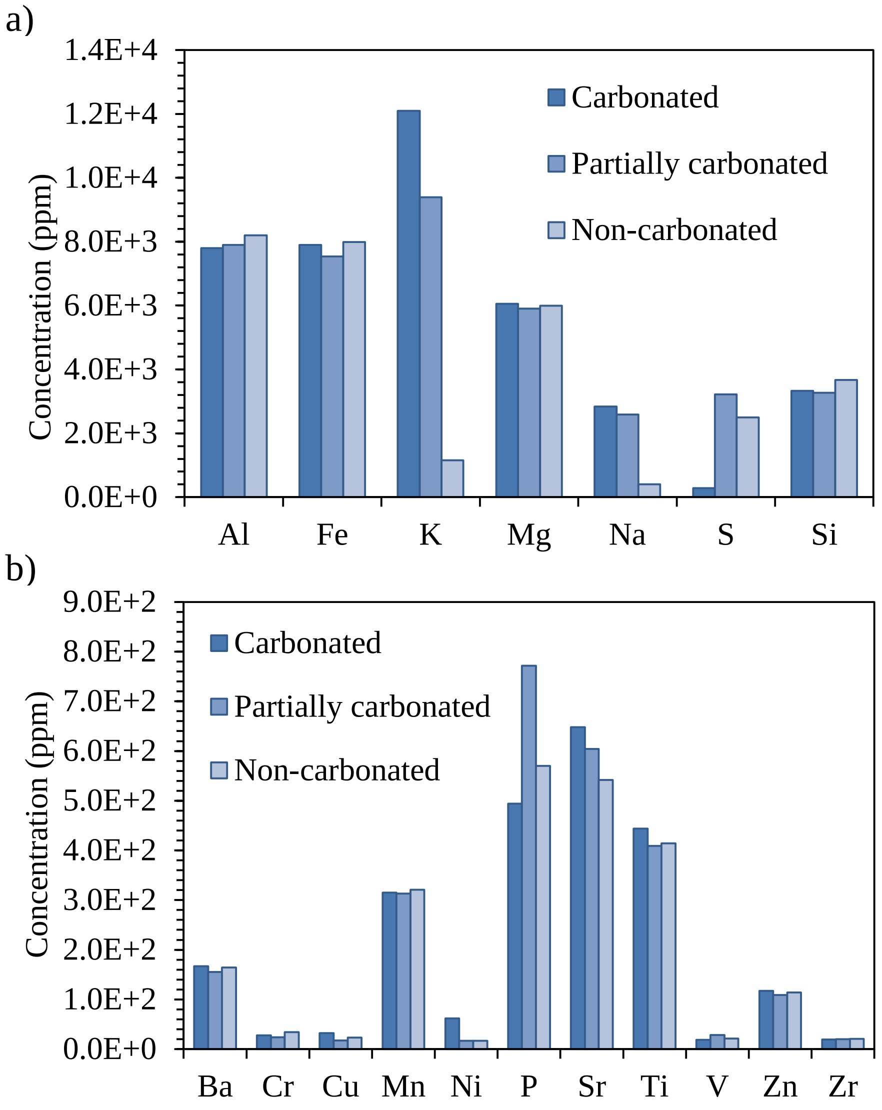

Figure 3. Results of the acid digestion of the samples **:** the charts show the elemental concentrations of (a) the major (excluding Ca, at ~3 x 10^5 ppm in all regions) and (b) the minor elements identified in the carbonated, partially carbonated and uncarbonated regions. Instrumental uncertainty in ICP-MS determinations is 2.5% in each concentration measurement shown.

Figure 4 shows LA-ICP-MS maps across the carbonated regions in Core 1. Two distinct regions with differing chemical compositions were observed: one at the reaction front (the carbonation front) and the other behind the carbonation front (visible as a transitional region of partial carbonation), indicating that carbonation did not occur in a single-step process at a well-defined single front. The carbonated region was depleted in Ca due to its release from C-S-H during the carbonation process [Morandeau *et al.*, 2014]) and was rich in Si; the decalcification of C-S-H is known to result in the formation of a highly-polymerised Si-rich gel [Fernández-Bertos *et al.*, 2004]. Si was present at lower concentration within the partially carbonated zone. The contents of Fe and Mg were similar in both the carbonated and uncarbonated regions, but both these elements were slightly depleted in the partially carbonated zone, which corresponds to the results obtained by acid digestion (Figure 3a). It is not immediately obvious from thermodynamic or solubility arguments why this should be the case, but this is a point worthy of further investigation in the future.

The most striking difference between regions of carbonated and non-carbonated NRVB shown in Figure 4 was the distribution of S, which was either depleted (carbonated region), low (non-carbonated region) or enriched (carbonation front). This is also reflected in the concentrations of S measured after acid digestion (Fig. 3a). Any S present is likely to exist in calcium aluminate hydrate phases (particularly ettringite and hydrated calcium (ferro) aluminate monosulphate (AFm)), which have low solubility at high pH but are unstable under lower pH conditions, such as those prevalent during carbonation (pH 7 – 8.5) [Morandeau *et al.*, 2014]. Therefore, any S present would likely dissolve upon carbonation, and migrate away from the carbonated region towards uncarbonated material. This same phenomenon was observed for Al and S, where there is an elevated concentration of these elements immediately ahead of the carbonation front and supports the hypothesis that ettringite or AFm phases decompose upon carbonation and Al migrates towards the uncarbonated material [Nishikawa *et al.*, 1992]. It is possible that other oxyanions, such as PO_4^{3-}, which are present in the calcium silicate phases of Portland Cement clinker and the interlayers of C-S-H [Poulson et al. 2010], may undergo a similar process, as evidenced by the apparent enrichment of P in the partially carbonated region and depletion in the carbonation, as shown in Figure 3

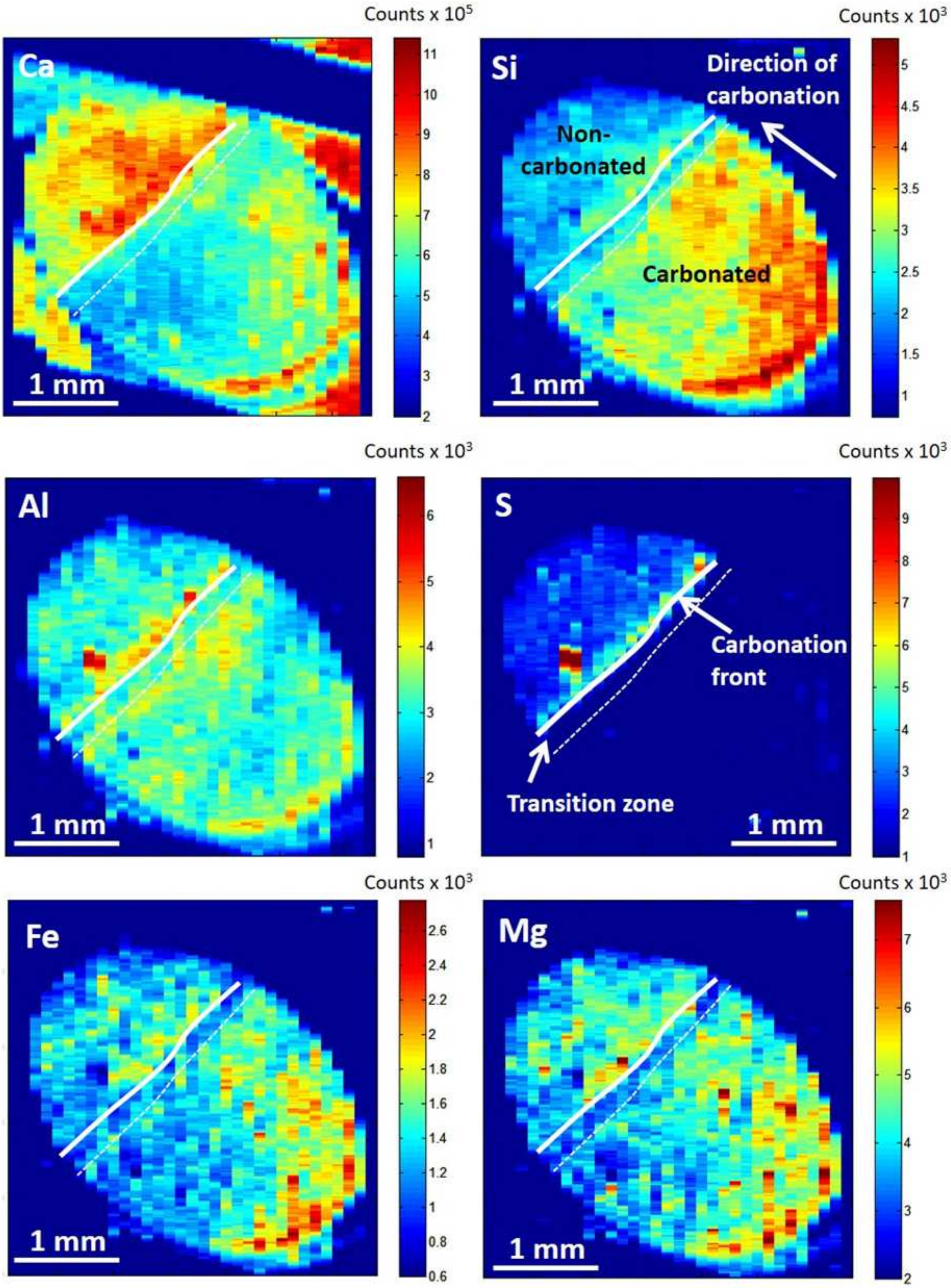

Figure 4. LA-ICP-MS maps showing the relative distribution of Ca, Si, Al, S, Fe and Pin the region immediately surrounding the carbonation front of Core 1.

Further elemental maps (Fig. 5) were acquired on a duplicate sample, taken from a region that was also measured using X-ray microtomography (see below). In agreement with the data presented in Figure 4, this sample also demonstrated a carbonation reaction front, however the determination of its location and the analysis of a partially carbonated zone was hampered by the presence of an unreacted particle of cement at the carbonation front (see Si, Al and S elemental maps, Figure 5) and also by the presence of a fracture (see Si, Na and K elemental maps, Figure 5). The distributions of elements were broadly consistent with those observed in Figure 4, giving further evidence for the decalcification of C-S-H in carbonated regions.

In agreement with the digest data for Na and K (Fig. 3), these elements were observed to be enriched in the carbonated region and depleted in the non-carbonated region. The concentration of Na and K was lower in the vicinity of the front; the implications of these observations will be explored in more detail in Section 4.

The contents of Fe and Mg were similar in both the carbonated and uncarbonated regions, but both these elements were slightly depleted in the partially carbonated zone, which corresponds to the results obtained by acid digestion (Figure 4). It is not immediately obvious from thermodynamic or solubility arguments why this should be the case, but this is a point worthy of further investigation in the future.

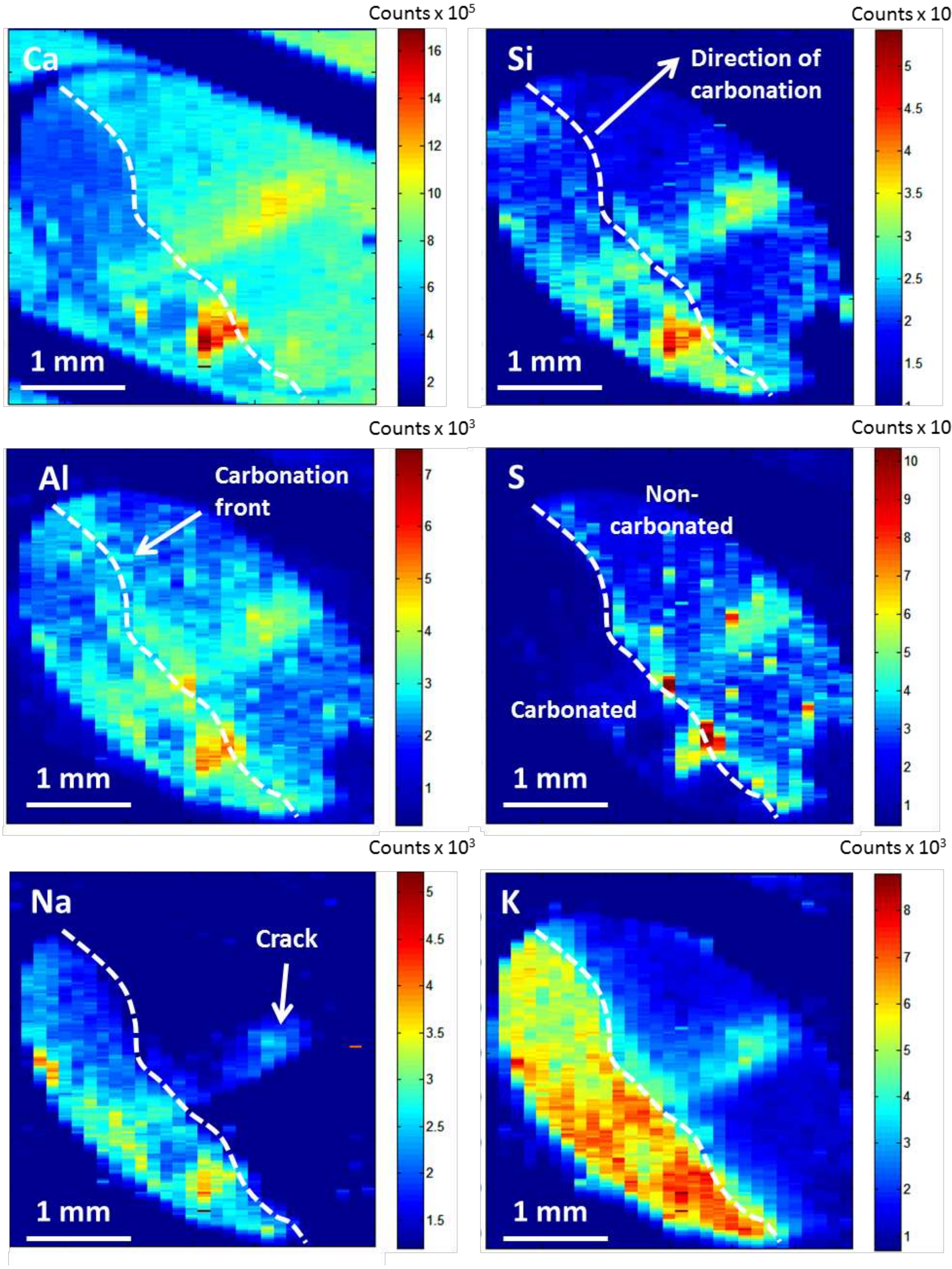

Figure 5. LA-ICP-MS maps showing the relative concentrations of Ca, Si, Al, S, Na and K in a partially carbonated sample of NRVB, corresponding to the region analysed by X-ray microtomography.

3.4 X-ray microtomography

Selected slices of the representative volume of interest (VOI, 601×601×601 voxels at 5 μm resolution) for samples assessed from Cores 1 and 3 are shown in Figure 6 The brightest isolated phase regions were assigned to unreacted Portland cement particles [Gallucci *et al.*, 2007]. In the case of the partially carbonated regions (Figure 6(b) and (e)) there was also a very bright feature corresponding to the accumulation of carbonation reaction products at the carbonation front. This difference in brightness indicates that the density of the carbonation front is higher than that of the other material. Voids appeared as darker areas [Gallucci *et al.*, 2007] and were clearly identified by their spherical morphology in all samples assessed. The carbonated regions (Figure 6a,d) show some streak-like features which may tentatively be identified as remnants left in the microstructure by the passage of the carbonation front; such features are not evident in the uncarbonated regions (Figure 6c,f).

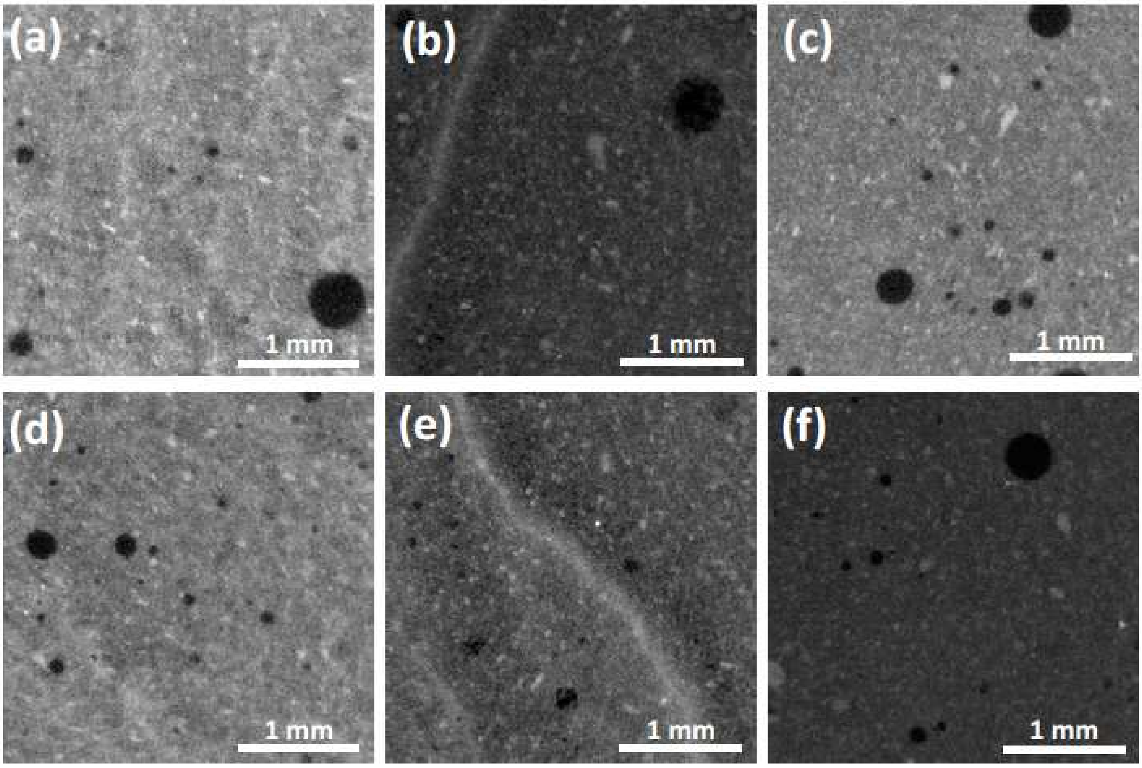

Figure 6. Selected slices through the VOIs in each region of core: (a) and (d) carbonated regions; (b) and (e) partially carbonated regions and; (c) and (f) uncarbonated regions, of Core 1 and 3 respectively.

2D images of selected slices, and 3D reconstructions of the VOI, of Core 3 are shown in Figures 7 and 8, respectively. The carbonated region (Fig. 7a) had a reduced fraction of pores compared to the uncarbonated region (Fig. 7c) due to the formation of calcium carbonate in the pore space. In the partially carbonated sample (Fig. 7b), at least two carbonation fronts were identified in the VOI selected. Although they are quite distinct, the formation of more than one front indicates that carbonation is neither occurring homogeneously throughout the sample, nor as a single-step process at one sharply defined carbonation front. The highest porosity was observed in the partially carbonated zone just behind the carbonation front.

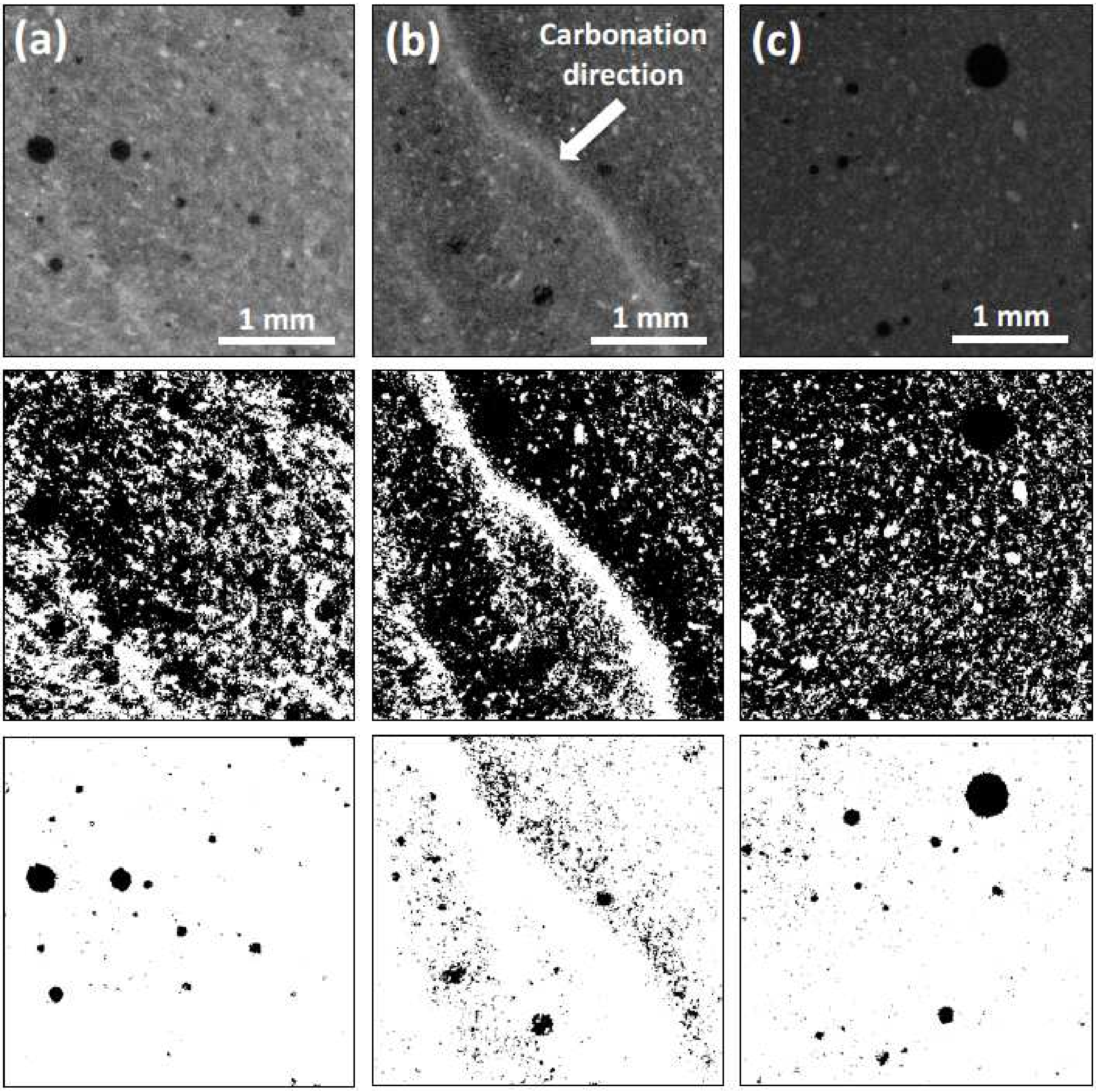

Figure 7. 2D VOI reconstructions of samples from Core 3. The top row shows grey scale images, the centre row the images segmented into solid (white) and pore (black) regions, and the bottom row the images segmented into areas of large pores (black)

of: (a) the carbonated region; (b) the partially carbonated region and; (c) the uncarbonated region.

The 3D reconstructions of the VOI (Fig. 8) indicate a higher fraction of large pores were present in the uncarbonated region (Fig. 8c) and that there was a high fraction of pores in the vicinity of the carbonation front, particularly just ahead of the very dense (bright) region in the sample (Fig. 8b).

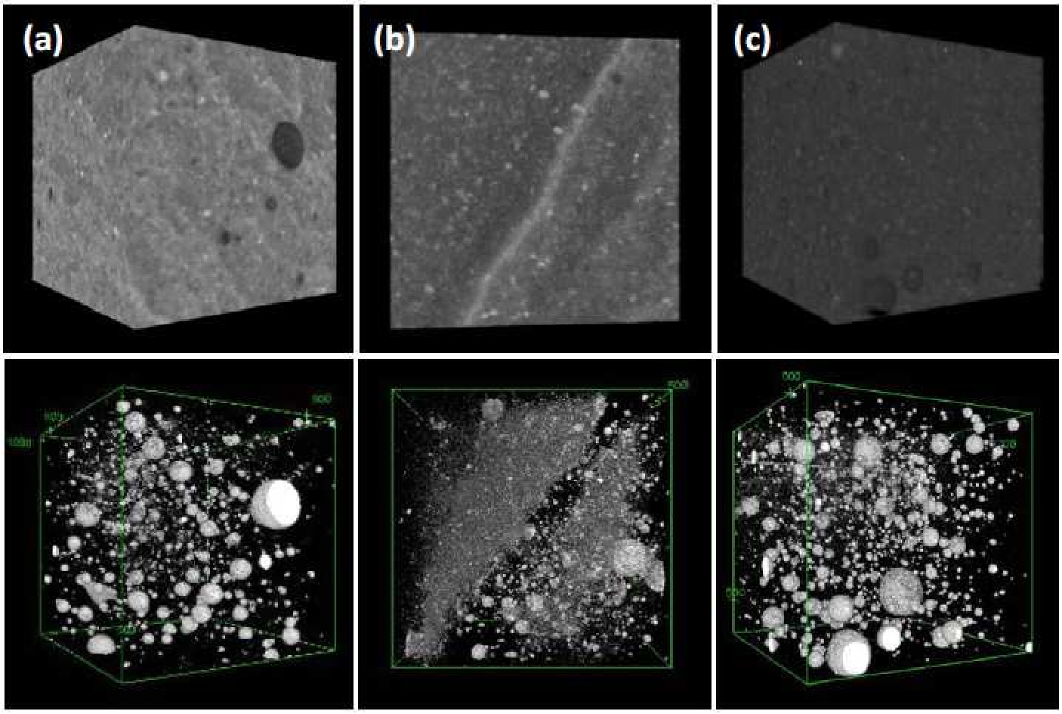

Figure 8. Sample from Core 3: (a) carbonated region; (b) partially carbonated region (carbonation is from top left corner) and; (c) the uncarbonated region. 3D reconstructions of the VOI (top row) and the VOI re-thresholded to show only the large pores (bottom row)

The porosity determined from analysis of this data for two samples from Cores 1 and 3 is summarised in Table 3. The average segmented porosity of the carbonated region is ~30% lower than that in the uncarbonated region, which confirms that carbonation products are precipitating in pore space, resulting in an increase in density.

.

Table 3. Summary of segmented porosity results

Core and Sample Number	Regions		
	Carbonated	Partially carbonated	Uncarbonated
1			
Sample 1	33.3	-	-
Sample 2	22.0	41.4	37.9
9			
Sample 1	36.5	-	-
Sample 2	31.7	43.2	43.5
Average	30.9	42.2	40.7
SD[1]	6.2	1.2	3.9

Notes: [1] – Standard deviation.

3.5 Raman spectroscopy

Despite leaving the samples to photobleach, all data recorded were detrimentally affected by fluorescence, leaving just the most intense bands visible. Portland cements are known to fluoresce [Richardson *et al.*, 2010], and so while not entirely unexpected, the fluorescence was more severe than had been anticipated.

All of the spectra obtained showed the characteristic ν_1 carbonate band at 1085 cm^{-1}, attributed to either calcite or aragonite [Black, 2009]. No evidence of any other calcium carbonate polymorphs, or of carboaluminate phases was observed. In some of the more well-defined spectra it was possible to see a lattice vibration band at 280 cm^{-1} or the ν_4 carbonate band at about 710 cm^{-1}; these bands are attributed to calcite. There was typically an increase in the intensity of the carbonate bands within the carbonated zone compared to regions beyond the carbonation front, indicating higher concentrations of carbonate within the carbonated zone. Similarly, in isolated spectra away from the carbonation front it was possible to discern a weak band at ~360 cm^{-1} attributed to portlandite. It was not possible to identify any other species within the spectra. Indeed, the region 900 – 1030 cm^{-1}, where characteristic sulfate ν_1 bands are expected, was examined closely, but no peaks were observed. This should not be taken as there having been no sulfate species present, but rather that fluorescence obscured any bands.

3.6 Mineralogical and elemental analysis

The distribution of major and minor elements was mapped using BSEM-EDXA for several regions of Core 1 closely matching those examined by other techniques. Data acquired across the principal carbonation front are presented in Figure 9, where a major change in the microstructure of the hardened grout upon carbonation can be observed. The decomposition of the fine-grained C-S-H gel matrix and the formation of a very fine-grained mixture of calcium carbonate and silica-rich material at a micron scale can be observed, accompanied by the development of very concentric fine shrinkage cracks cemented by secondary calcium carbonate. This in agreement with other experiments on the carbonation of NRVB and other Portland cements [*e.g.* Rochelle and Milodowski, 2013].

In agreement with LA-ICP-MS results, the EDXA elemental maps recorded across the main carbonation reaction front (Figure 8) show that carbonation resulted in significant chemical changes and movement of major chemical components. In particular, K and, to a lesser extent, Na were concentrated within the altered cement matrix behind the main carbonation front. Ca was strongly concentrated at the reaction front and S was depleted from the carbonated region behind the main reaction front, but enriched in the relatively unaltered region. Sulphur was particularly concentrated immediately ahead of the main carbonation front where the calcium carbonate precipitation was found to be dominant. In the uncarbonated region ahead of the reaction front, localized high concentrations of S, Al and Ca were observed in some samples, particularly in large voids created by air-bubbles entrained within the grout during mixing, which would allow the expansive formation of ettringite. Chlorine was present in the epoxy-resin used during sample preparation, so the map for Cl is a proxy for the resin-impregnated micro-porosity within the grout. The elemental maps across the reaction front show that Cl was markedly depleted within the carbonated front compared to the remaining microstructure, suggesting a lower porosity and higher density in this region. This reduction in porosity is likely to result from the precipitation of calcium carbonate within the main porosity of the reaction front.

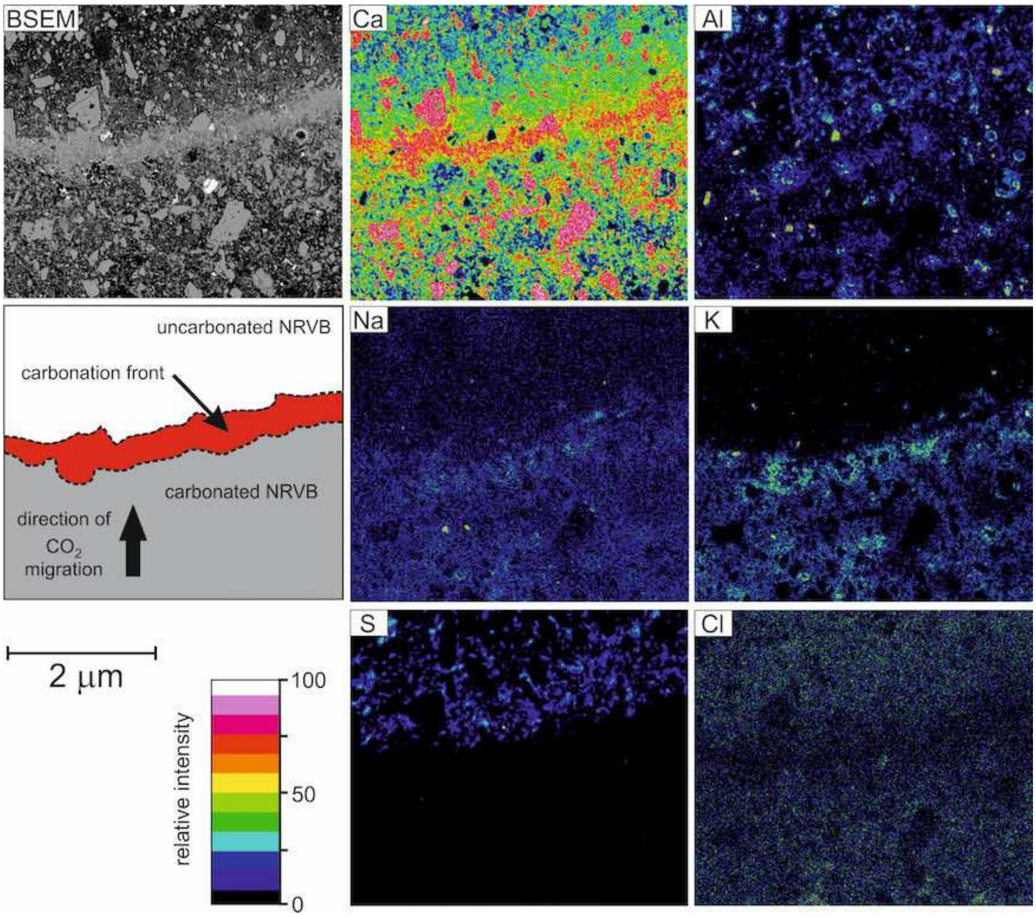

Figure 9. BSEM image with corresponding colour-contoured relative-intensity EDXA element distribution maps, recorded from a polished thin section prepared across the carbonation reaction front for Core 1.

Areas far ahead of the carbonation front were also mapped, and showed that the cement paste had not undergone intense alteration when compared to the grout within, and behind, the main alteration front. In these regions C-S-H, calcium aluminate hydrates, and partially hydrated cement clinker particles were still present. However, some carbonation of the portlandite and C-S-H gel in these regions had clearly occurred (Figure 10). Although “primary” calcium carbonate is present in the NRVB as limestone flour added during the preparation of the NRVB cement, these limestone particles are readily distinguished petrographically from the secondary calcium carbonate produced by cement carbonation. The limestone flour particles are characterized by angular fragments of calcium carbonate disseminated throughout the NRVB samples (Figure 10). In contrast, secondary calcium carbonate formed by carbonation reaction is manifested as fine-grained secondary calcium carbonate forming alteration fringes around the margins of portlandite crystals or in irregular patches replacing C-S-H matrix material (Figure 10). Secondary calcium carbonate was also sometimes observed nucleating around limestone flour fragments. EDXA analyses and X-ray maps show that the secondary calcium carbonate forms fringes around portlandite crystals (Figure 10). Semi-quantitative compositional estimates from EDXA show the secondary carbonate fringes have a Ca:O atomic ratio (~0.3) similar to that of the limestone fragments (Ca:O ~0.34), implying that the carbonation reaction product is essentially $CaCO_3$ (Ca:O = 0.33). In contrast, the relatively unaltered cores of the partially-carbonated portlandite crystals have a much higher Ca:O atomic ratios that vary between calcium carbonate (0.33) and portlandite (0.5). The armouring of the surface of these portlandite crystals by a reaction rim of secondary calcium carbonate will probably have protected or limited reaction with CO_2 to some extent.

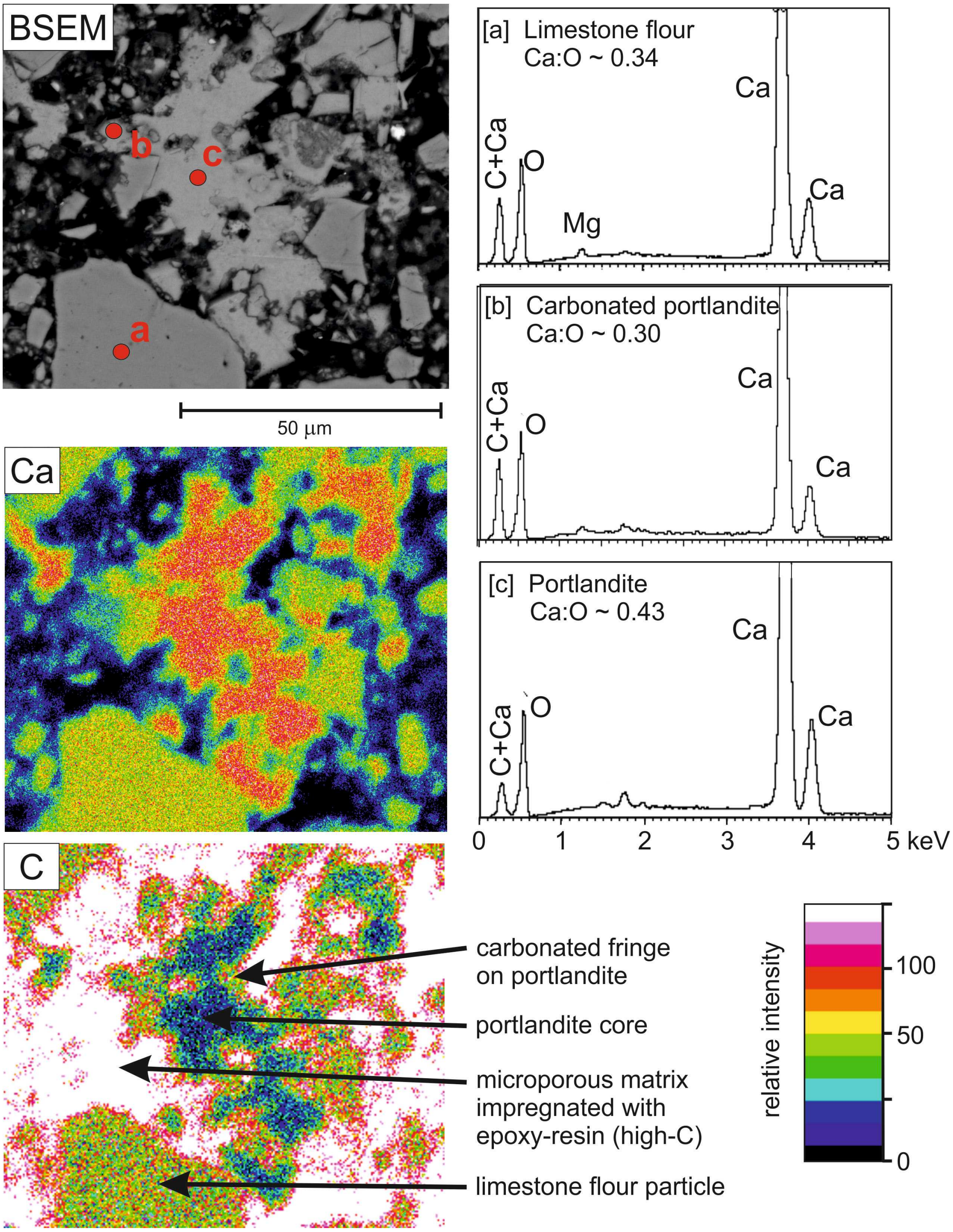

Figure 10. BSEM image with corresponding colour-contoured relative-intensity EDXA element distribution maps for Ca and C, showing angular fragments of limestone flour, and the development of a calcium carbonate alteration fringe around a patch of portlandite nucleated within the hydrated cement matrix. Example EDXA spectra are also illustrated for: (a) a primary limestone flour particle; (b) the carbonated reaction fringe around portlandite, and; (c) the relatively unaltered core of the portlandite. . Recorded from a polished thin polished thin section No.3 prepared

100 mm from the vent inlet, and 90 mm ahead of the carbonation front, for Core 1 (Figure 2).

3.7 XRD analysis

The concentrations of crystalline phases in each of the cores, and each of the carbonation zones were determined (Table 4).

The main crystalline phase present in all samples was calcite ($CaCO_3$) with smaller amounts of aragonite ($CaCO_3$), dolomite ($CaMg(CO_3)_2$), portlandite ($Ca(OH)_2$), gypsum ($CaSO_4.2H_2O$) and quartz (SiO_2) also detected. The very small amounts of quartz and dolomite are unlikely to have formed during cement hydration and carbonation, and most probably represent impurities in the limestone additive used in the NRVB. Petrographic observations confirmed the presence of fine fragments of crushed quartz and dolomite. Minor reflections were also tentatively identified for ettringite ($Ca_6Al_2(SO_4)_3(OH)_{12}.26H_2O$, where the main reflection is at ~9.6Å) and a broad reflection with a *d*-spacing of 7.78Å that may indicate the presence of calcium monocarboaluminate ($Ca_4Al_2(CO_3)(OH)_{12}.5H_2O$, which has a characteristic diffraction peak at around 7.6Å (cf. Lothenbach et al., 2008). The calcium monocarboaluminate appears to be present throughout the cores and may represent a reaction product formed with the limestone flour, which would be consistent with other studies that have previously shown that calcium mono- and hemicarboaluminate ($Ca_4Al_2(CO_3)_{0.5}(OH)_{13}.5.5H_2O$) phases form in hydrated blended cements containing limestone additives (Matschei et al., 2007; Lothenbach et al., 2008). Calcium hemicarboaluminate was not identified in the present study on carbonated NRVB. However, its absence is not inconsistent with the observations of Lothenbach et al (*op. cit.*) who observed that both mono- and hemicarboaluminate formed after 2 to 7 days, the monocarboaluminate content then increased with time, whilst hemicarbonate disappeared after 14 days.

Other minor weak reflections at ~14 and ~7.1Å were also identified that may represent C-S-H phases (e.g. Biagioni et al., 2015). However, the identity of these phases could not be confirmed. No calcium monosulphoaluminate phases were found in the post-experimental NRVB. However, Lothenbach et al. (2008) also found the

AFm phases to have very poor crystallinity, and with variable compositions, making them difficult to detect by XRD analysis.

Table 4. Summary of quantitative XRD results for crystalline components in Cores 1, 2 and 3 (normalised to 100%)

Core	Vertical distance from inlet vent(cm)	Relative mineral proportions (wt % normalised to 100%)[1]							Other minor phases[2]	Portlandite : total $CaCO_3$ (calcite +aragonite) ratio	Relationship to petrographically-defined carbonation reaction front
		Calcite	Aragonite	Dolomite	Portlandite	Ettringite	Gypsum	Quartz			
1	0.1	96.7		0.7		1.9		0.6	Mono. 7.1 Å	0.000	Carbonated zone
	0.7	96.6		0.6		1.8		1.0	Mono. 7.1 Å	0.000	Carbonated zone
	0.9	97.2				1.8		1.0	Mono. 7.1 Å	0.000	Main carbonation reaction font
	30.7	85.1	9.7		4.0			1.2	Mono. 7.1 Å	0.042	Relatively unaltered NRVB distant from reaction front
	48.8	83.8	8.9		5.2			2.1	Mono. 7.1 Å	0.056	Relatively unaltered NRVB distant from reaction front
3	0.2	91.8	-	0.6	-	-	2.4	<0.5	Mono. 7.1 Å	0.000	Carbonated zone
	0.6	90.8	-	0.6	-	-	2.2	0.9	Mono. 7.1 Å	0.000	Main carbonation reaction font
	1.2	82.3	3.1	<0.5	1.8	2.6	3.1	1	Mono. 7.1 Å	0.021	Matrix immediately in front of reaction front
	20.0	73.2	9	-	5	3.2	-	0.9	Mono. 7.1 Å	0.061	Relatively unaltered NRVB distant from reaction front
	44.8	74.4	7.6	-	5.3	3.1	-	1.1	Mono. 7.1 Å	0.065	Relatively unaltered NRVB distant from reaction front
2	0.1	93.6	-	0.6	-	-	-	<0.5	Mono. 14.1 Å	0.000	Carbonated zone

	0.5	90.7	-	0.6	<0.5	2.3	-	0.9	Mono. 14.1 Å	0.000	Main carbonation reaction font
	0.7	60.2	-	-	24	7.7	-	0.8	Mono. 14.1 Å	0.399	Relatively unaltered NRVB distant from reaction front
	21.5	61.9	-	-	22.5	4	3.9	<0.5	Mono. 14.1 Å	0.363	Relatively unaltered NRVB distant from reaction front
	41.5	60	-	-	23.4	4.1	4.1	0.7	Mono. 14.1 Å	0.390	Relatively unaltered NRVB distant from reaction front

Notes:

[1] Normalisation excludes quantification of minor calcium monocarboaluminate and unidentified 7.1 Å and ~14 Å phases.

[2] “Mono.” = calcium monocarboaluminate; “7.1 Å” = unidentified phase; “14 Å” = unidentified phase.

Quantification of the absolute composition of the NRVB samples by XRD is problematic. Petrographic observations indicate that there is a significant amount of C-S-H and AFm material present in the largely unaltered cement matrix ahead of the main carbonation front. These phases are disordered or amorphous, and are not easily detectable by XRD. Therefore, the quantitative XRD data presented in Table 4 only represent the “relative” proportions of the crystalline phases present. This, together with a large proportion of the calcite present representing original limestone flour additive, means that the extent of carbonation cannot be evaluated simply from the total relative amounts of calcite and aragonite alone. However, because carbonation involves the replacement of portlandite (as well as C-S-H) by calcium carbonate (as shown by petrographic analysis), the amount of portlandite relative to the total amount of calcium carbonate (calcite + aragonite) should provide an indicator of how deep carbonation has occurred in the grout.

The portlandite : total $CaCO_3$ ratios based on the XRD results is presented in Table 4. The detection of portlandite is a key marker of regions that are not yet fully carbonated, and appears to correlate with the radial distance of the sample from the centre of the vent. The XRD data show that portlandite has completely reacted to form calcium carbonates within the reaction front and the main carbonated zone behind this front. The relatively unaltered cement ahead of the main reaction front still contains significant portlandite. However, the portlandite : total $CaCO_3$ ratios progressively increase with increasing distance from this front. This implies that carbonation has occurred in the cement ahead of the main reaction front (where complete carbonation has occurred) but that this diminishes with increasing distance. This is consistent with the BSEM-EDXA petrographic observations, which showed patchily-distributed secondary fine-grained calcium carbonate replacing and armouring portlandite and C-S-H in the cement matrix ahead of the main reaction front (see previous discussion in Section 3.6 and illustrated in Figure 10.

Core 2 appeared to be anomalous, compared to cores 1 and 3, with respect to the portlandite content of the relatively unaltered grout. The amount of portlandite preserved in this core appears to be significantly higher than the other two cores, and may reflect some degree of heterogeneity of carbonation within the experimental waste drum.

Aragonite was identified within the uncarbonated material ahead of the main reaction front, but is absent in the main carbonated grout regions. Aragonite is metastable and unlikely to have been present in the original limestone flour additive. Therefore, the aragonite is likely to be a reaction product in the cement, and may provide some further indication of depth of penetration and reaction of CO_2 ahead of the main carbonation front. It would appear that, if aragonite had formed initially within the main carbonated zone, it has subsequently been replaced by calcite as the degree of carbonation alteration progressed.

In terms of the minor mineral phases, quartz and dolomite are present within the limestone flour used in the grout. Gypsum, ettringite and calcium monocarboaluminate are likely to be secondary precipitates formed during the hydration of the cement in the grout. These minor phases could not generally be discriminated during petrographic analysis (BSEM-EDXA) because of their low concentration, their fine grain size and the intimate mixing of the hydrated cement phases. However, discrete coarse crystals of ettringite were observed in large voids in the hardened grout that represent air bubbles that were originally entrained in the cement paste during mixing, and that were previously occupied by air or water. There was no obvious relationship between the distributions of these minor phases and the carbonation front.

4. Discussion

Using LA-ICP-MS, micro-tomography and EDXA, three distinct regions were identified in each sample, 1) carbonated, 2) partially carbonated and 3) uncarbonated. A carbonation front and a partially carbonated zone were identified in the partially carbonated region. Analysis by LA-ICP-MS and EDXA showed that K and Na were concentrated within the carbonated regions behind the main reaction front, and the concentration was greatest in a narrow zone up to 1-2mm wide immediately behind where the Ca was concentrated within the main reaction front. The carbonation front was enriched in S and Al, and the former was depleted from the carbonated region at, and behind, the main reaction front. Micro-tomography results indicated that the porosity of the carbonated region was lower than in the uncarbonated region, due to deposition of secondary calcium carbonate within the pore space of the hardened grout (as confirmed by BSEM/EDX); however, micro-permeametry results showed that the grout was more permeable in the carbonated region. This higher permeability may be due to greater interconnectivity of micro-fractures within the pore network.

Similar porosity results to those obtained here have been reported by Hills *et al.* [1999], who used SEM to identify a porosity reduction of up to 26% in hardened cemented wasteforms subjected to accelerated carbonation. Lange *et al.* [1996] have also reported increased mechanical strength in carbonated cement wasteforms, which they associated with the precipitation of calcium carbonate products in the specimen pores, and an increase in density and reduction of the total porosity. The porosity of the partially carbonated region is similar to that of the uncarbonated region, and Figures 7 and 8 show that there is an increase in porosity near to the carbonation front.

The higher permeability of the carbonated regions when investigated by micro-permeametry appears at first to contradict the petrographic observations and the X-ray micro-tomography results, which indicate that the porosity of the carbonated zone is reduced in comparison to the unaltered cement. However, this may be because the micro-porosity in the carbonated cement is more interconnected than in the unaltered cement matrix. The petrographic analysis showed the presence of micro-fractures in the carbonated region (described as fine shrinkage cracks), and whilst these micro-fractures largely appeared to be cemented by secondary calcium carbonate reaction product, the presence of some uncemented micro-fractures may provide a network of higher permeability pathways within the altered cement.

The LA-ICP-MS results suggest that alkali ions are released from the cement component of the NRVB during the hydration of the PC powder, and become distributed between the aqueous solution and the precipitating C-S-H phases [cf. Lothenbach *et al.*, 2008]. The results shown here suggest that the carbonation of C-S-H phases corresponds to enhanced alkali concentrations, evidenced by the higher concentration of Na and K in the carbonated regions of the samples. In their study of the carbonation of PC pastes, Anstice *et al.* [2005] reported a decrease in Na and K concentration in the pore solution extracted from carbonated samples *cf.* uncarbonated material, which is the opposite of the results presented here. They postulated that this was due to enhanced binding of alkali metals to the solid products of carbonation, which they stated was most likely to be by the hydrous silica gel formed during decalcification of C-S-H. Because the concentrations of Na and K were lower in the immediate vicinity of the carbonation front in this work, it may be hypothesised that either 1) C-S-H carbonation is not the main process that occurs in the vicinity of the carbonation front (which would be consistent with the fact that the large additional quantity of $Ca(OH)_2$ contributed to the NRVB by the slaked lime component of its formulation must also carbonate, compared to the much lower content formed in Portland cement hydration), or 2) that C-S-H carbonation is slower in this region. These may be the reasons why the interfacial region at the carbonation front in this work has a higher porosity than the carbonated region.

The results from the X-ray micro-tomography studies warrant further discussion. In a recent study, Morandeau *et al.* [2014] evaluated the carbonation of pure Portland cement binders *via* a gamma ray attenuation method (GRAM), and also identified a reduction in the total porosity of carbonated specimens; however, they observed densification in the vicinity of the surface where carbonation seemed to be most predominant, which differs from the results observed in this study. The discrepancy between that study and the NRVB results reported here could be associated with differences in the chemistry of NRVB and hydrated Portland cement only as noted above, leading to differences in the kinetics of carbonation of the reaction products forming in these binders, or the differences in resolution of GRAM *vs.* micro-tomography, so that the increase in the porosity near the carbonation front could not be detected by GRAM. It has been proposed [Villain *et al.*, 2007] that under natural carbonation conditions, the carbonation of portlandite and C-S-H occurs simultaneously, even though from a thermodynamic perspective carbonation of portlandite prevails over C-S-H carbonation [Glasser and Matschei, 2007]. Morandeau *et al.* [2014] have observed that the initial rates of carbonation of these phases are comparable, but while carbonation of C-S-H continues to take place, the carbonation of portlandite reduces, possibly due to the armouring of the portlandite discussed earlier, and stops during the time of CO_2 exposure.

Additionally, it was proposed [Morandeau *et al.*, 2014] that the carbonation of C-S-H is the main contributor to pore clogging, with the effects depending on its Ca/Si ratio, while dissolution of portlandite via carbonation can increase the porosity to partially counteract the pore-blocking effects of $CaCO_3$ precipitation. Considering this, it is likely that dissolution of calcium hydroxide, along with carbonation of ettringite and AFm phases, with a limited extent of decalcification of the C-S-H phases, could be taking place in the vicinity of the carbonation front, thereby reducing the precipitation of carbonation product in the pores of this region. This hypothesis is consistent with the LA-ICP-MS results, where a reduced concentration of alkalis in the non-carbonated cement immediately ahead of the carbonation front was observed, where higher concentrations of alkalis were associated with their potential binding to solid carbonation products and the hydrous silica gel forming during decalcification of C-S-H in this area. This observation is consistent with the BSEM and EDXA observations.

The conditions used to induce carbonation also have a significant impact on how this phenomenon proceeds, and therefore it is important to consider that the NRVB evaluated in this study was carbonated under conditions of high CO_2 pressure, when compared to the 1-4kPa partial pressure used in most cement/concrete carbonation tests (with the exception of 100% CO_2 or supercritical conditions used in occasional specialised work). Under those conditions, the carbonation of the C-S-H phase is known to prevail over carbonation of calcium hydroxide [da Silva *et al*, 2009] as a consequence of the formation of crystalline calcium carbonate on the surface of the calcium hydroxide, inhibiting its further dissolution [Hidalgo *et al.*, 2008; García-González *et al.*, 2006]. Densification of samples carbonated under high CO_2 pressures has been identified, consistent with the theory of pore clogging due to carbonation of C-S-H as suggested by Morandeau *et al.* [2014]. This further supports the hypothesis that in the vicinity of the carbonation front of the NRVB evaluated, dissolution of portlandite via carbonation to produce calcium carbonate, along with limited decalcification of C-S-H, are the main degradation processes taking place in this region.

In analysing the XRD results further, it is relevant to discuss the following points in more detail. There is significant formation of secondary calcium carbonate behind the main reaction front (defined by the extent of phenolphthalein staining as shown in Table 4), and within the main carbonated region behind the reaction front, nearly all the portlandite, C-S-H and calcium (sulfo)aluminate hydrate phases are replaced by calcite. Calcite is the principal carbonate phase precipitated, although a small amount of aragonite is sometimes present.

This study also demonstrates that the impact of carbonation extends well beyond the apparent limit of reaction indicated by phenolphthalein staining, and reaction has occurred throughout the sample. Even in the regions furthest from the centre of the vent, where phenolphthalein staining suggests that carbonation has not taken place, the XRD and petrographic observations show that portlandite and C-S-H have partially-reacted with CO_2 to produce secondary calcium carbonates. This is reflected in the portlandite : $CaCO_3$ ratio, which progressively decreases with increasing distance from the reaction front, and by the presence of portlandite crystals armoured by reaction rims of $CaCO_3$ in the “relatively unaltered” cement. The XRD and petrographic results clearly indicate that the extent of carbonation is underestimated by phenolphthalein staining. The petrographic observations clearly showed the growth of secondary calcite within the partially carbonated grout matrix. Petrographically, it is possible to differentiate between the calcite originally present in the limestone flour and the secondary calcite formed from the carbonation of other phases, and this supports the observations made using XRD. Finally, there appears to be a distinct relationship between the amount of carbonation and the radial proximity to the centre of the vent; material closest to the vent has been carbonated more than material further away from the vent.

The complete carbonation of the cement phases of the backfill that are in close proximity to the carbon dioxide is to be expected, since one of the roles of the phases such as portlandite, calcium silicate hydrate and calcium aluminate hydrate are to react to reduce the migration of $^{14}CO_2$.

Of greater importance is that some carbonation occurs throughout the sample, indicating that migration and reaction of the carbon dioxide is not restricted to the fully carbonated zone only but also extends deeper into the cement beyond this reaction front. This may impact on understanding and modelling the migration and retardation of $^{14}CO_2$ derived from ^{14}C-bearing wastes in the GDF and the development of the safety case.

5. Conclusions

The main conclusions resulting from this work are:

- For the high lime and limestone with Portland cement NRVB grouts, while carbonation leads to the formation of a distinct carbonation front, there was clear evidence of partial carbonation occurring well beyond the main reaction front.
- Three distinct regions were identified in the hardened NRVB grouts; carbonated, partially carbonated and uncarbonated. Within the partially carbonated region, a carbonation front and a partially carbonated zone were discerned.
- K, and to a lesser extent Na, were concentrated within a 1-2 mm deep zone in the carbonated region just behind the main reaction front.
- The area just ahead of the carbonation front was enriched in both S and Al, and S is depleted from the carbonated material behind the main reaction front.
- Within the main carbonated region, virtually all of the hydrated cement phases (portlandite, calcium silicate hydrate and calcium aluminate hydrate) were carbonated and calcite was the predominant phase. Aragonite was also formed,

but this appears to be initially formed ahead of the main reaction front, and was possibly destabilized, replaced and altered to calcite as more extensive carbonation proceeds.

- Some carbonation had occurred throughout the sample. Even within material indicated by phenolphthalein solution to be uncarbonated, partial carbonation had occurred.
- The porosity of the carbonated grout is lower than in the uncarbonated material due to replacement of pore space with precipitated calcium carbonate. However, the highest porosity was observed in the partially carbonated region.

6. Acknowledgements

The authors acknowledge the contribution of S Williams at Radioactive Waste Management in funding the experimental work that led to the preparation of this paper. The X-ray microtomography work was conducted at the Manchester X-ray Imaging Facility, and the authors thank the technical staff of that facility for their assistance in scanning the samples and calculating reconstructions. We thank Neil Bramall for assistance with LA-ICP-MS measurements. AEM, LPF, SJK, IM and AB publish with the permission of the Executive Director of the British Geological Survey (NERC). CLC is grateful to EPSRC for the award of an ECR Fellowship (EP/N017374/1). Portions of this work were performed at the MIDAS Facility, at the University of Sheffield, which was established with support from the Department of Energy and Climate Change.

References

Amec Foster Wheeler. 2017. “Screening limit” on the rate of gas generation from individual intermediate-level waste packages. Amec Foster Wheeler Report, SA/ENV-0888 Issue 3, 41pp.

Anstice, D. J., Page, C. L., Page, M. M., 2005. The pore solution phase of carbonated cement pastes. Cem. Concr. Res. 35, 377-383.

Biagioni, C., Merlino, S., Bonaccorsi, E. 2015. The tobermorite supergroup: a new nomenclature. Mineralogical Magazine, 79, 485-495.

Bamforth, P.B., Baston, G.M.N., Berry, J.A., Glasser, F.P., Heath, T.G., Jackson, C.P., Savage, D. and Swanton, S.W. 2012. Cement materials for use as backfill, sealing and structural materials in geological disposal concepts. A review of current status. Serco Report, SERCO/005125/001 Issue 3. Nuclear Decommissioning Authority, Harwell, UK. 235pp

Black, L., 2009. Raman spectroscopy of cementitious materials. In: J. Yarwood, R. Douthwaite, S. Duckett, (editors), Spectroscopic Properties of Inorganic and Organometallic Compounds, 40, Royal Society of Chemistry, UK, 72-127.

BSI, BS 594-1:2005, Hot rolled asphalt for roads and other paved areas. Specification for constituent materials and asphalt mixtures, British Standards Institution, 2005.

BSI, BS EN 459-1:2015, Building lime. Definitions, specifications and conformity criteria, British Standards Institution, April 2015.

Cann, G. C., Orr, R. M., 2010. A technical specification for Portland cement, blast furnace slag and fly ash for use in the encapsulation/immobilisation of radioactive waste materials (8th Revision), NNL 10653.

da Silva FG, Helene P, Castro-Borges P, Liborio JBL (2009) Sources of variations when comparing concrete carbonation results. J Mater Civ Eng 21(7):333-342.

Department of Energy and Climate Change (DECC), Implementing Geological Disposal, A Framework for the long-term management of higher activity radioactive waste, July 2014

Fernández-Bertos, M., Simons, S. J. R., Hills, C. D., Carey, P. J., 2004. A review of accelerated carbonation technology in the treatment of cement-based materials and sequestration of CO_2. J. Hazard. Mater. B112, 193-205.

Francis, A. J., Cather, R., Crossland, I. G., 1997. Development of the Nirex Reference Vault Backfill; Report on Current Status in 1994, S/97/014.

Gallucci, E., Scrivener, K., Groso, A., Stampanoni, M., Margaritondo, G., 2007. 3D experimental investigation of the microstructure of cement pastes using synchrotron X-ray microtomography (μCT). Cem. Concr. Res. 37, 360-368.

García-González, C. A., Hidalgo, A., Andrade, C., Cruz Alonso, M., Fraile, J., López-Periago, A. M., Domingo, C., 2006. Modification of composition and microstructure of Portland cement pastes as a result of natural and supercritical carbonation procedures. Industrial Engineering Chemistry Res. 45, 4985-4992.

Glasser, F., Matschei. T., 2007. Interactions between Portland cement and carbon dioxide. in: Proceedings of the 12th International Congress on the Chemistry of Cement. Montreal, Canada.

Harris, A. W., Boult, K. A., Manning, M. C., Tearle, W. M., 2003a. Experimental study of carbon dioxide uptake by NRVB and 3:1 BFS/OPC, Serco Report Serco/ERRA-0453.

Harris, A. W., Manning, M., Tearle, W. M., 2003b. Carbonation of Nirex Reference Vault Backfill, SERCO/ERRA-0454.

Hidalgo, A., Domingo, C., Garcia, C., Petit, S., Andrade, C., Alonso, C., 2008. Microstructural changes induced in Portland cement-based materials due to natural and supercritical carbonation. J. Mater. Science, 43, 3101-3111.

Hills, C. D., Sweeney, R. E. H., Buenfeld, N. R., 1999. Microstructural study of carbonated cement-solidified synthetic heavy metal waste. Waste Management 19, 325-331.

Hoch, A.R., Rochelle, C.A., Humphreys, P.N., Lloyd, J.R., Heath, T.G. and Thatcher, K.E. 2016. Carbon-14 Project Phase 2. Formation of a Gas Phase and its Migration. Amec Report, AMEC/200047/007, Issue 1, 189pp.

Hoffmann, U., Stipp, S. L. S., 1998. Preliminary results on the behaviour of Ni(II) in the calcite-water system, Mineralogical Magazine 62A, 642-643.

Johannesson, B., Utgenannt, P., 2001. Microstructural changes caused by carbonation of cement mortar. Cem. Concr. Res. 31, 925-931.

Kutchko, B.G., Strazisar, B.R., Dzombak, D.A., Lowry, G.V. and Thaulow, N., 2007. Degradation of well cement by CO2 under geological sequestration conditions, Environmental Science and Technology 41, 4787-4792.

Lange, L. C., Hills, C. D., Poole, A. B., 1996. The effect of accelerated carbonation on the properties of cement-solidified waste forms. Waste Management 16, 757-763.

Lange, L. C., Hills, C. D., Poole, A. B., 1997. Effect of carbonation on properties of blended and non-blended cement solidified waste forms. J. Hazard. Mater. 52, 193-212.

Lothenbach, B., Le Saout, G., Gallucci, E., Scrivener, K., 2008. Influence of limestone on the hydration of Portland cements. Cem. Concr. Res. 38, 848-860.

Matschei, T., Lothenbach, B., Glasser, F.P. 2007. The role of calcium carbonate in cement hydration. Cem. Concr. Res., 37, 551-558

Milodowski, A.E., Rochelle, C.A., Lacinska, A. and Wagner, D. 2011. A natural analogue study of CO_2-cement interaction: Carbonation of calcium silicate hydratebearing rocks from Northern Ireland. Energy Procedia, 4, 5235-5242.

Morandeau, A., Thiéry, M., Dangla, P., 2014. Investigation of the carbonation mechanism of CH and CSH in terms of kinetics, microstructure changes and moisture properties. Cem. Concr. Res. 56, 153-170.

Nishikawa, T., Suzuki, K., Ito, S., 1992. Decomposition of synthesized ettringite by carbonation. Cem. Concr. Res. 22, 6-14.

Nuclear Decommissioning Authority. 2010. Generic Disposal System Technical Specification. NDA Report NDA/RWMD/044. Nuclear Decommissioning Authority, Harwell.

Pitty, A. and Alexander, R. (editors). Maqarin Phase IV Report: A joint-funded international project report between NDA RWMD, Andra, CEA, SKB. Nagra and JNC. Published by the Nuclear Decommissioning Authority, 2011 Moor Row, Cumbria, United Kingdom, 381pp.

Poulsen, S. L., Jakobsen, H. J., Skibsted, J., 2010. Incorporation of phosphorus guest ions in the calcium silicate phases of Portland cement from 31P MAS NMR spectroscopy. Inorg. Chemistry 49, 5522-5529.

Provis, J. L., Myers, R. J., White, C. E., Rose, V., van Deventer, J., 2012. X-ray microtomography shows pore structure and tortuosity in alkali-activated binders. Cem. Concr. Res. 42, 855-864.

Purser, G., Milodowski, A.E., Noy, D.J., Rochelle, C.A., Harrington, J.F., Butcher A. and Wagner, D. 2015. Modification to the flow properties of repository cement as a result of carbonation. In: Shaw, R.P. (editor). Gas Generation and Migration in Deep Geological Waste Repositories. Geological Society, London, Special Publications, 415, 35-46.

Pusch R. Yong R.N. and Nakano M., Geologic Disposal of Low- and Intermediate-Level Radioactive Waste, CRC Press, 2017

Radioactive Waste Management Limited. 2016a, Geological Disposal: Gas Status Report. *Nuclear Decommissioning Authority Report*, DSSC/455/01, 126pp (ISBN 978-1-84029-568-9).

Radioactive Waste Management Limited. 2016b, Geological Disposal Waste Package Evolution Status Report, DSSC/451/01, 291pp (ISBN 978-1-84029-564-1)

Richardson, I. G., Skibsted, J., Black, L., Kirkpatrick, R. J., 2010. Characterisation of cement hydrate phases by TEM, NMR and Raman spectroscopy. Adv. Cem. Res. 22, 233-248.

Rochelle, C.A., Milodowski, A.E., Lacinska, A., Richardson, C., Shaw, R., Taylor, H., Wagner, D., Bateman, K., Lécolier, E., Ferrer, N., Lamy, F., Jacquemet, N., Shi, Ji-Q, Durucvan, S. and Syed, A.S. 2009. JRAP-14: Reactions between CO2 and borehole infrastructure. Deliverable JRAP-14/3: Report on Laboratory Experiments and Modelling. European Commission FP6 Project Number SES6-CT-2004-502816, Network of Excellence on Geological Storage of CO_2 (CO2GeoNet). 138pp.

Rochelle, C. A., Milodowski, A. E., 2013. Carbonation of borehole seals: comparing evidence from short-term laboratory experiments and long-term natural analogues. Appl. Geochemistry 30, 161-177.

Rochelle, C.A., Purser, G., Milodowski, A.E., Noy, D.J., Wagner, D., Butcher, A. and Harrington, J.F. 2013. CO_2 migration and reaction in cementitious repositories: A summary of work conducted as part of the FORGE project. British Geological Survey Open Report, OR/13/004. 30pp.

Shafique, M., Walton, J., Gutierrez, N., Smith, R., Tarquin, A., 1998. Influence of carbonation on leaching of cementitious wasteforms. J. Environmental Engineering 124, 463-467.

Snyder, R. L., Bish, D. L., 1989. Quantitative analysis. In: D. L. Bish, J. E. Post, (editors), Modern Powder Diffraction, Reviews in Mineralogy, Volume 20, Mineralogical Society of America, USA, 101-144.

Sun, J., 2010. Carbonation Kinetics of Cementitious Materials Used in the Geological Disposal of Radioactive Waste, PhD thesis, University of London.

Vasconcelos R. G. W., Beaudoin N., Hamilton A., Hyatt N. C., Provis J. L. and Corkhill C. L. Characterisation of a high pH cement backfill for the geological disposal of nuclear waste: The Nirex Reference Vault Backfill. Applied Geochemistry, 89, 180 – 189 (2018).

Villain, G., Thiery, M., Platret, G., 2007. Measurement methods of carbonation profiles in concrete: thermogravimetry, chemical analysis and gammadensimetry. Cem. Concr. Res. 37, 1182-1192.

Wilson, J.C., Benbow, S.J., Metcalfe, R., Savage, D., Walker, C.S. and Chittenden, N. 2011. Fully coupled modeling of long term cement well seal stability in the presence of CO_2, Energy Procedia, 4, 5162-5169.

Wilson, J., Benbow, S. and Metcalfe, R. 2017. Understanding the long-term evolution of cement backfills: alteration of NRVB due to reaction with groundwater solutes. Radioactive Waste Management Report, RWM/03/043, 132pp.

Živica, V., Bajza, A., 2001. Acidic attack of cement based materials — a review: Part 1. Principle of acidic attack. Constr. Build. Mater. 15, 331-340.